CrossMark

ORIGINAL PAPER

# Electrochemical performance of the rare-earth perovskite-type oxide $La_{0.6}Sr_{0.4}Co_{0.2}Fe_{0.8}O_3$ as negative electrode material for Ni/oxide rechargeable batteries

**John Henao[1] · Oscar Sotelo[1] · Maura Casales[1] · Lorenzo Martinez-Gomez[1]**

© The Author(s) 2017. This article is an open access publication

**Abstract** In this paper, the perovskite-type oxide $La_{0.6}Sr_{0.4}Co_{0.2}Fe_{0.8}O_3$ was evaluated as a novel negative electrode material for Ni/oxide rechargeable batteries. The structure and morphology of the as-prepared powder was studied by scanning electron microscopy and X-ray diffraction. The electrochemical performance of the perovskite-type oxide was investigated using chronopotentiometric, chronoamperometric and potentiodynamic polarization techniques. The maximum discharge capacity values of the perovskite-type electrodes were obtained during the first three cycles (51, 172 and 462 mAh g$^{-1}$ at 298, 313 and 333 K, respectively). The maximum adsorption capability of hydrogen in the perovskite-type electrode was 1.72% wt. hydrogen at a current rate of 125 mA g$^{-1}$, 333 K and 6 M KOH. The cycling ability was fairly good with 64% capacity conservation after 20 cycles at 333 K. The electrochemical evaluation was also performed using different electrolyte concentrations; interestingly, the maximum discharge capacity of the perovskite-type electrodes increased in a linear-like manner with the incremental changes in electrolyte concentration. The hydrogen diffusion coefficient and exchange current density were also estimated to discuss the kinetics of the process.

✉ John Henao
  jhenao.icf.unam@gmail.com

[1] Instituto de Ciencias Físicas, Universidad Nacional Autónoma de México (UNAM), Avenida Universidad s/n, 62210 Cuernavaca, Morelos, Mexico

## Introduction

Nickel metal hydride (Ni/MH) batteries are one type of eco-friendly energy systems that have shown key technology advantages for applications in many fields [1, 2]. In these systems, hydrogen storage properties of active materials determine the amount of stored energy and their cycle life. Since the introduction of commercial Ni/MH batteries in the late 1980s, many different intermetallic compounds have been evaluated as anode materials in Ni/MH batteries due to their ability to form metal hydrides [3, 4]. The AB$_5$-type intermetallic alloys have been often employed in commercial batteries because of their good electrochemical capacities (around 330 mAh g$^{-1}$) [5, 6]. However, in recent years, researchers' efforts have been focused on finding new types of negative electrode materials to replace conventional intermetallic ones [7–9]. The reasons for such efforts include the high fabrication cost of conventional alloys, electrochemical degradation at high temperatures and poor high-rate dischargeability.

One of the applications of Ni/MH batteries is actually linked to the military industry and industrial machinery, both of which require rechargeable batteries to work satisfactorily at high temperatures (from 313 to 353 K) [10, 11]. Since AB$_5$-based alloys present their best performance in a temperature range between 293 and 313 K [12], engineers have proposed various types of materials as alternatives to the intermetallic ones. In this manner, rare-earth perovskite-type oxides (REMeO$_3$, in which RE = a rare-earth element and Me = a transition metal) have risen as a new kind of material for negative electrodes in Ni/MH batteries [13]. REMeO$_3$ are known not only for having proton conductivity at high temperatures and under hydrogen atmospheres, but also for their superior hydrogen solubility over other metal oxides. Using perovskite-type

oxides is also advantageous because of their abundance and lower fabrication costs than seen with conventional inter-metallic alloys [14].

In the last decade, rare-earth perovskite-type oxides have shown many key aspects that have supported their development and application as negative electrode mate-rials for the next generation of Ni/MH batteries. Since the metal hydride electrode in Ni/MH batteries can be substi-tuted for the perovskite-type oxide electrode, this new technology has been given the name Ni/oxide battery. Among the different perovskite-type compounds studied as negative electrode materials for Ni/oxide rechargeable batteries [13], $LaFeO_3$ perovskite-based oxides have shown promising electrochemical performance (capacity values of around 350 mAh $g^{-1}$ at 333 K) [13, 15]. Nevertheless, there are various key points concerning these oxides that are still under investigation. For instance, their poor intrinsic conductivity leads to higher resistance during the charge transfer process. In addition to the conductivity issues, the hydrogen diffusion coefficient presents low values when compared with those of intermetallic com-pounds. Recently, various solutions have been proposed to improve these weak points [16–18]. One of the attempts for improving the electrochemical performance of the oxide electrodes was the introduction of dopant elements within the perovskite structure. For example, Deng et al. [19] reported a discharge capacity value of around 502 mAh $g^{-1}$ with a current density of 31.25 mA $g^{-1}$ at 333 K for the $La_{1-x}Sr_xFeO_3$ (for $x = 0.4$) oxide electrode, which is considerably much higher than that reported for the undoped $LaFeO_3$ and $AB_5$ alloys [5, 6, 13]. Another option for improving the electrochemical performance of perovskites was the reduction of the particle size of the powder (from micrometric to nanometric scale) [16]. This alternative has been demonstrated to enhance the charge transfer process at the electrode's surface. As a result, the discharge capacity of the nanometric $LaFeO_3$ was improved by 38% with respect to the same micrometric powder. Thus, using both dopant elements and nanometric powders may be a good choice to build up perovskite-type negative electrodes for Ni/oxide rechargeable batteries.

In the present work, a doped $LaFeO_3$ perovskite-type oxide ($La_{0.6}Sr_{0.4}Co_{0.2}Fe_{0.8}O_3$) with a nano-sized particle distribution was successfully used for the preparation of negative electrodes for Ni/oxide rechargeable batteries. The aim of this study was to evaluate the performance of the $La_{0.6}Sr_{0.4}Co_{0.2}Fe_{0.8}O_3$ oxide electrode at various elec-trolyte concentrations and at various temperatures. The structure, morphology, and kinetics of the electrochemical process were systematically investigated to explain the performance of the proposed rare-earth perovskite-type composition.

## Experimental

### Powder characterization

Commercial $La_{0.6}Sr_{0.4}Co_{0.2}Fe_{0.8}O_3$ perovskite-type oxide powder (99.9% purity, Aldrich) was used as active material to build up the negative electrodes in the present study. X-ray diffraction (XRD) was performed on a Bruker D8 Advance diffractometer equipped with a monochromatic Cu Kα X-ray source ($k = 1.5418$ Å; 40 kV) and positional detector (LYNXEYE™ 1D with an active length of 2.7522°). XRD patterns were collected at room tempera-ture over the angular range of $20° \leq 2\theta \leq 80°$ with a step size of 0.008° and measuring time of 300 s per step. Scanning electron microscopy (SEM) analysis was carried out in a TESCAN MIRA3 LMU scanning microscope to investigate the morphology and particle size of the initial powder. The characterization of the initial powder was also conducted using a laser diffraction equipment (LS 1057083 Laser Diffraction, Malvern Instruments) to reveal the par-ticle size distribution.

### Electrochemical measurements

The working electrode for electrochemical measurements was prepared with the mixture of $La_{0.6}Sr_{0.4}Co_{0.2}Fe_{0.8}O_3$ powder and a binder (70% PTFE + 30% carbon black) in a weight ratio of 1:1. The mixture was ground in a mortar for 1 h and then cold pressed over an Ni-grid current collector under a pressure of 47 MPa, forming an electrode pellet of 11.3 mm in diameter. Electrochemical measurements were performed using a potentiostat/galvanostat test instrument (Gamry Instruments, Interface 1000E) with an open two-electrode cell configuration at 298, 313 and 333 K. $Ni(OH)_2/NiOOH$ (99.9% purity, Aldrich) was used as a counter electrode, while KOH 6, 7.5, 8.5, 10 and 12 M aqueous solutions were used as electrolyte. During the charge–discharge processes, the electrodes were fully charged for 4 h at a specific current density of 125 mA $g^{-1}$ and discharged at the same specific current density to the cutoff potential of $-0.4$ V (versus $Ni(OH)_2/NiOOH$ ref-erence electrode). The standing time between charge and discharge was set to 600 s.

The kinetic measurements, linear polarization and chronoamperometry of perovskite-type electrodes were performed on an open three-electrode cell configuration consisting of a working electrode ($La_{0.6}Sr_{0.4}Co_{0.2}Fe_{0.8}O_3$ electrodes), a counter electrode ($Ni(OH)_2/NiOOH$) and a reference electrode (Hg/HgO). The linear polarization curves were obtained by scanning the electrode potential at the rate of 0.1 mV/s from $-6$ to $+6$ mV versus the open circuit potential (OCP) for the different electrolyte

concentrations at 0% depth of discharge (DOD) and at 298 K. The chronoamperometry tests were carried out by applying an overpotential of +600 mV at 0% DOD. The current transient curves were recorded following the potential step for the different electrolyte concentrations and 298 K.

## Results and discussion

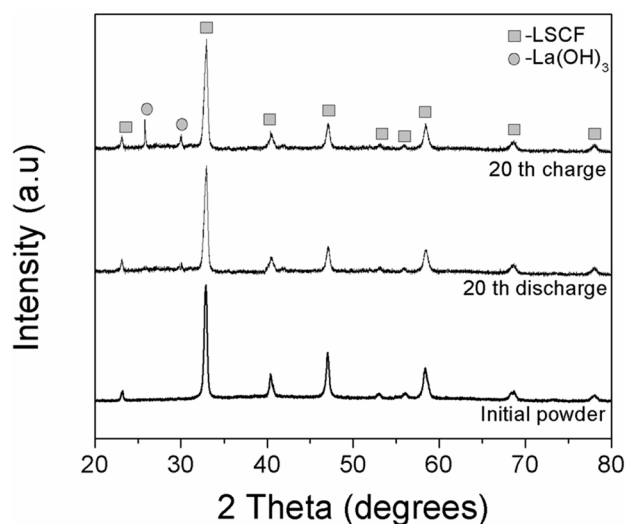### Morphological and structural characterization

The real particle size distribution of the initial powder was analyzed by LS as shown in Fig. 1a. The particle size of the $La_{0.6}Sr_{0.4}Co_{0.2}Fe_{0.8}O_3$ was distributed in the range of 380–1300 nm, and the average particle size was about 712 nm. Scanning electron microscopy analysis (see
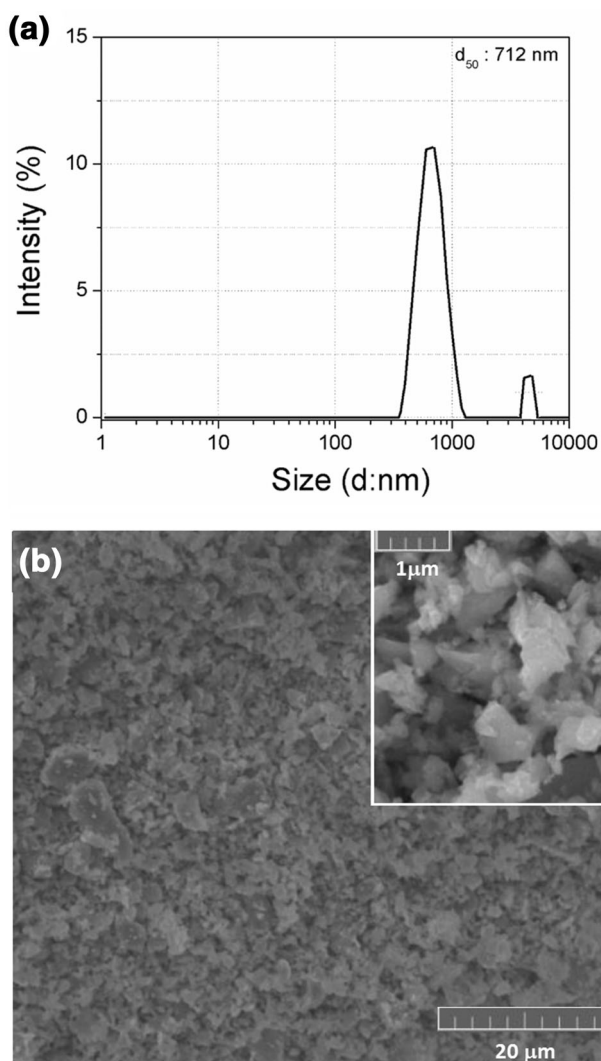


Fig. 1b) revealed that $La_{0.6}Sr_{0.4}Co_{0.2}Fe_{0.8}O_3$ particles displayed an irregular morphology and were agglomerated with each other. Considering the application, it is always an advantage to use of ultrafine oxides over bulk ones, since the diffusion path of both hydrogen ions and electrons can be shortened using ultrafine particles as demonstrated in previous studies [13, 16].

The XRD analyses were carried out to characterize the phase structure of the $La_{0.6}Sr_{0.4}Co_{0.2}Fe_{0.8}O_3$ electrodes at different states (uncharged, charged and discharged); the recorded XRD patterns are shown in Fig. 2. The XRD pattern for the as-prepared electrode did not reveal the presence of additional diffraction peaks attributed to secondary phases or reaction products. Despite the presence of the binder material in the as-prepared electrode, the peaks corresponding to the perovskite phase were clearly identifiable. The $La_{0.6}Sr_{0.4}Co_{0.2}Fe_{0.8}O_3$ electrodes display an orthorhombic phase (space group R3c). The calculated lattice parameters of the perovskite-type oxide $La_{0.6}Sr_{0.4}Co_{0.2}Fe_{0.8}O_3$ at the initial state (see Table 1) were obtained by Rietveld refinement using the MAUD software. The calculated experimental lattice parameters are similar to the theoretical lattice parameter for the perovskite-type oxide $La_{0.6}Sr_{0.4}Co_{0.2}Fe_{0.8}O_3$ ($a_{theoretical} = 5.4451$ Å and $c_{theoretical} = 13.2553$ Å, corresponding to the JCPDS # 48-0124 card). The XRD patterns after charging and discharging (Fig. 1) revealed that $La_{0.6}Sr_{0.4}Co_{0.2}Fe_{0.8}O_3$ electrodes kept their perovskite-type structure and showed no signs of secondary phases. However, the calculated lattice parameters of the cycled electrodes changed with respect to the as-prepared ones. Consequently, the cell volume experienced an expansion of 0.32 and 0.35% after the 20th discharge and 20th charge cycle, respectively.



**Fig. 1** **a** LS curve for the initial $La_{0.6}Sr_{0.4}Co_{0.2}Fe_{0.8}O_3$ powder, **b** SEM micrograph of the initial powder

**Fig. 2** XRD patterns of the as-prepared $La_{0.6}Sr_{0.4}Co_{0.2}Fe_{0.8}O_3$ electrode and after 20 galvanostatic charge/discharge cycles in KOH 6 M at 298 K

**Table 1** Lattice parameters of $La_{0.6}Sr_{0.4}Co_{0.2}Fe_{0.8}O_3$ (LSCF) electrodes from Rietveld's method

| Sample | Crystallographic system | Lattice parameters (Å) | | Cell volume (Å$^3$) | $\Delta v/v$ (%) | $R_{wp}$ (%) | $\chi^2$ |
|---|---|---|---|---|---|---|---|
| | | $a$ | $c$ | | | | |
| LSCF-as-prepared | Rhombohedral | 5.448 (0.003) | 13.256 (0.003) | 340.731 (0.006) | * | 3.26 | 1.38 |
| LSCF-20th-discharge | Rhombohedral | 5.458 (0.002) | 13.249 (0.001) | 341.806 (0.003) | 0.32 | 1.72 | 1.09 |
| LSCF-20th-charge | Rhombohedral | 5.459 (0.003) | 13.248 (0.004) | 341.906 (0.007) | 0.35 | 2.53 | 1.15 |

Error values are reported in parentheses. $R_{wp}$ and $\chi^2$ are quality parameters of Rietveld refinement

*Reference volume

Interestingly, the obvious expansion of the cell volume in the perovskite-type electrodes is small in comparison to the volumetric expansion experienced by traditional inter-metallic alloys (up to 25% volume change) [20]. The change in the cell volume is attributed to the nature of the hydrogen uptake in perovskites [13]. Unlike conventional metal hydride alloys, in a perovskite, the dissociated $H_2O$ molecule, specifically $H^+$ proton, fills lattice positions associated with oxygen ions, producing interstitial ion defects. Since the $H^+$ proton is a bare ion without an electron cloud and has a tiny dimension, it will effectively interact with the valence electron density of the nearest neighbors, i.e., in oxide compounds the electron band gap restricts the interaction of the protons with the nearest electron clouds. Thus, the protons must be located inside the electron shell of the atom associated with them, i.e., the equilibrium position is fixed in the valence electron density of the oxygen [21, 22]. In contrast, in metal alloys, the $H^+$ protons attain their equilibrium positions within interstitial sites (octahedral and tetrahedral sites), because electrons are delocalized in the whole crystal, i.e., protons have the conduction band as their neighbor which allows protons to have a high coordination number [23]. Therefore, the fact that $H^+$ protons do not occupy the interstitial sites within the perovskite structure results in a smaller lattice expansion compared to the lattice expansion in metal hydride alloys. Similar lattice expansion values (<1%) of perovskite compounds after hydrogenation have also been reported in previous studies [19, 24].

### Electrochemical characterization

The electrochemical performance of the $La_{0.6}Sr_{0.4}Co_{0.2}Fe_{0.8}O_3$ electrode as a function of temperature was investigated by performing galvanostatic measurements. The charge–discharge cycle number as a function of the discharge capacity is shown in Fig. 3. Interestingly, the maximum discharge capacity of the $La_{0.6}Sr_{0.4}Co_{0.2}Fe_{0.8}O_3$ electrode was obtained during the first cycle at all of the tested temperatures. In this manner, the present results reveal that perovskite-type $La_{0.6}Sr_{0.4}Co_{0.2}Fe_{0.8}O_3$ electrodes can be discharged directly without previous
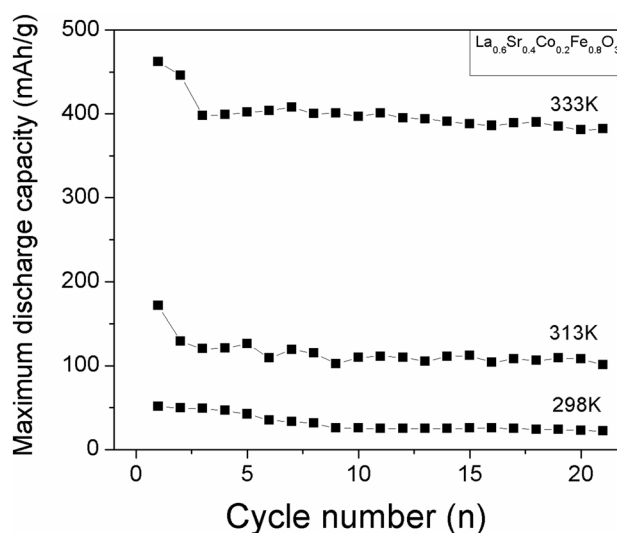


**Fig. 3** Discharge capacity vs cycle number at 298, 313 and 333 K in KOH 6 M, respectively. (discharge current density of 125 mA g$^{-1}$)

activation. This behavior has also been reported for other perovskite-type compounds such as $LaCrO_3$ and $LaGaO_3$, indicating that perovskite-type oxides do not require pre-treatments for electrochemical hydrogen storage. Of course, this situation is an advantage of the perovskite-type oxides over the intermetallic compounds, since the intermetallic compounds require more than three activation cycles for hydrogen uptake [25].
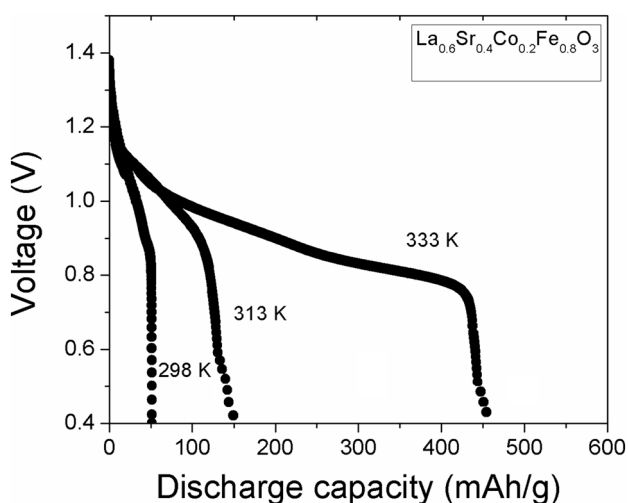
At 298 K, the discharge capacity of $La_{0.6}Sr_{0.4}Co_{0.2}Fe_{0.8}O_3$ electrode slightly decreased over the number of cycles from 51.4 to 21.9 mAh g$^{-1}$ after 20 cycles; see Fig. 3. When the temperature was increased to 313 and 333 K, the maximum discharge capacity of the electrodes increased. Experimental maximum discharge capacity values were 172 and 462 mAh g$^{-1}$ at 313 and 333 K, respectively, corresponding to 0.64 and 1.72% wt. of hydrogen. However, these capacity values declined during the first three cycles. Despite the steep decrease of the discharge capacity after the first cycles, Fig. 3, this compound conserves a good stable lifetime during long cycling. The cycling stability of the compound was estimated from the discharge capacity value after stabilization ($C_s$) by the

maximum discharge capacity value ($C_{max}$) according to the following equation [9]:

$$S_s = \frac{100 \times C_s}{C_{max}}. \tag{1}$$

The values of the discharge capacity conservation ($S_s$) were 47, 61 and 85% for the $La_{0.6}Sr_{0.4}Co_{0.2}Fe_{0.8}O_3$ electrode at 298, 313 and 333 K, respectively. Overall, the oxide electrode presented a good capacity retention, which is consistent with the stability presented for other perovskite-type compounds in previous studies [15, 26].
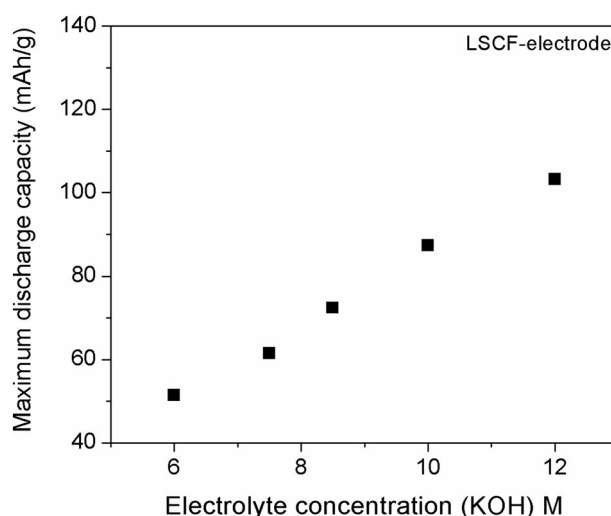
The maximum discharge capacity curves of the $La_{0.6}Sr_{0.4}Co_{0.2}Fe_{0.8}O_3$ electrodes at various temperatures are plotted in Fig. 4. The oxide electrode delivers a maximum discharge capacity (51.4 mAh g$^{-1}$) at 298 K, which was higher than that of the oxide electrode tested at 313 K (172 mAh g$^{-1}$) and at 333 K (462 mAh g$^{-1}$). This significant enhancement is attributed to several factors: (1) the improved atomic motion at the electrode/electrolyte interface; (2) the known resistance to corrosion of perovskite-type oxides; and (3) the increased phonon vibration promoted by the increase in temperature, which reduces the activation energy for hydrogen ion diffusion [13, 21]. The discharge capacity curves showed a horizontal potential plateau, and their extent increased with the temperature. This can be attributed to the stability of the structure, the combination of corrosion properties, and the mechanisms of ion migration in the unit cell of these compounds, in which protons are inserted into the oxygen vacancy sites and jump over these positions. The temperature increase then favors the insertion and movement of hydrogen ions. Interestingly, in the present work, the capacity values of the $La_{0.6}Sr_{0.4}Co_{0.2}Fe_{0.8}O_3$ electrodes are remarkably higher than the values reported for the $La_{0.6}Sr_{0.4}FeO_3$ in previous studies (70 and 350 mAh g$^{-1}$ for 298 and 333 K at 125 mA g$^{-1}$, respectively) [13, 18]. This finding is thought to be associated with the promotion of oxygen vacancies due to the use of Co as the dopant in the perovskite-type $La_{0.6}Sr_{0.4}FeO_3$ composition, thus resulting in an enhancement of the electrochemical capacity.

Following the study of the electrochemical performance of the oxide electrodes at various temperatures, the effect of increasing the electrolyte concentration on the oxide electrode performance was systematically investigated. Figure 5 shows the influence of electrolyte concentration on the discharge capacity of the perovskite-type electrode at 298 K. Interestingly, the discharge capacity of the electrode increases monotonously with the increase of the KOH concentration. This behavior is remarkably different from that of conventional intermetallic alloys in which higher electrolyte concentration is harmful for their electrochemical performance [27]. In intermetallic alloys, the accentuated corrosion of the alloy in highly concentrated KOH electrolyte promotes degradation of the discharge capacity. However, in the perovskite-type oxides, the electrochemical capacity increases because of the intrinsic corrosion resistance of this compound in highly concentrated alkaline media [13]. As a result, the increase in hydroxide ions content in the electrolyte also increases the possibility for hydrogen atoms to enter within the perovskite structure, which is reflected in an improved electrochemical capacity, i.e., the formation of water molecules takes place at the positive electrode due to a reaction of hydroxide ions with nickel hydroxide; concurrently, hydrogen protons are formed at the negative electrode due to the splitting of water.
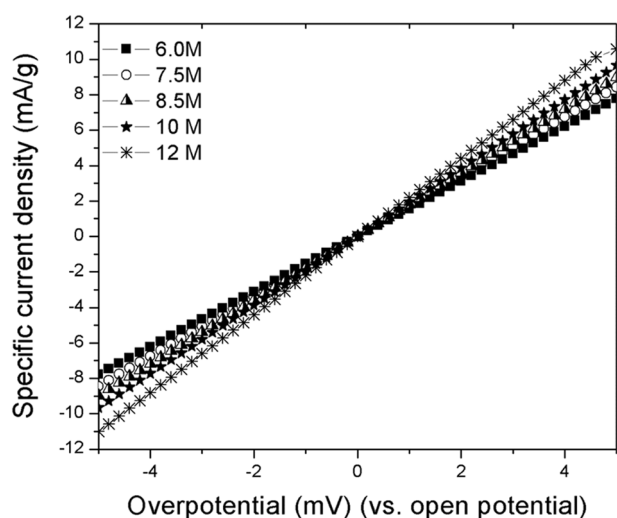


**Fig. 4** Discharge capacity curves at 298, 313 and 333 K in KOH 6 M, respectively. (discharge current density of 125 mA g$^{-1}$)



**Fig. 5** Maximum specific discharge capacity of the $La_{0.6}Sr_{0.4}Co_{0.2}Fe_{0.8}O_3$ electrode after galvanostatic cycling at various electrolyte concentrations and 298 K. (discharge current density of 125 mA g$^{-1}$)

**Fig. 6** Linear polarization curves of the $La_{0.6}Sr_{0.4}Co_{0.2}Fe_{0.8}O_3$ electrode at various electrolyte concentrations and 298 K

Figure 6 shows the linear polarization curves of the perovskite-type electrodes in different electrolyte concentrations. In this case, linear polarization technique involves the hydrogen reduction/oxidation reactions on the surface layer of the oxide electrode, and therefore the charge transfer rate at the electrode surface can be evaluated by the exchange current density ($I_0$) calculated from the following equation [28]:

$$I_0 = \frac{IT}{FR_p}, \tag{2}$$

where $R$ is the gas constant (J mol$^{-1}$K$^{-1}$), $T$ the absolute temperature (K), $F$ the Faraday constant (C mol$^{-1}$) and $R_p$ the polarization resistance (m$\Omega$) which is the reciprocal of the slope in the linear polarization curve. The exchange current density is a powerful parameter that can be used as a measure of the kinetics of the electrochemical hydrogen reaction since it is related to the electrocatalytic activity of the charge transfer reaction on the surface of the electrode. Interestingly, the reaction resistance of the $La_{0.6}Sr_{0.4}Co_{0.2}Fe_{0.8}O_3$ electrode decreased when the concentration of the electrolyte increased; this can be observed from the slope of the curves shown in Fig. 6. Consequently, the exchange current density increased with the increase in electrolyte concentration, which can be attributed to the

enhancement of the charge transfer process at the electrode surface. These results are summarized in Table 2.

Figure 7 shows the semi-logarithmic curves of anodic current vs. time response of the $La_{0.6}Sr_{0.4}Co_{0.2}Fe_{0.8}O_3$ electrode at 0% DOD and different KOH electrolyte concentrations. These curves are obtained following the application of a constant step potential while monitoring the current–time response. Each curve has two parts, the first one at the early stage where the polarization current drastically decreases, and a second part where the decreasing trend of the current becomes moderate. It is then in the second region in which the surface concentration of hydrogen protons approaches zero and the electrode reaction becomes controlled by proton diffusion. Based on the solution of the diffusion equation for a constant step potential, the proton hydrogen diffusion coefficient $D_H$ can be calculated according to the following equation [29]:

$$\log i = \log\left[\frac{6FD_H}{da^2}(C_0 - C_s)\right] - \frac{\pi^2}{2.303}\frac{D_Ht}{a^2}, \tag{3}$$

where $i$, $D$, $d$, $a$, $C_0$, $C_s$ and $t$ represent anodic current density (mA g$^{-1}$), hydrogen diffusion coefficient (cm$^2$ s$^{-1}$), density of the oxide (g cm$^{-3}$), radius of the oxide particles, initial hydrogen concentration in the bulk of the electrode (mol cm$^{-3}$), surface hydrogen concentration of the alloys (mol cm$^{-3}$) and discharge time (s), respectively. Thus, $D_H$ can be calculated from the slope of the second region of the log $i$ against time curve if the mean particle size diameter of the oxide electrode is known. In the present case, as determined experimentally in "Morphological and structural characterization", the value of $a$ was 356 nm. The calculated values of $D_H$ for the $La_{0.6}Sr_{0.4}Co_{0.2}Fe_{0.8}O_3$ electrode in different KOH electrolyte concentrations are listed in Table 2. It can be seen that the hydrogen diffusion rate of the oxide electrode is $1.87 \times 10^{-14}$ cm$^2$ s$^{-1}$ in 6 M KOH and $2.14 \times 10^{-14}$ cm$^2$ s$^{-1}$ in 12 M KOH. Considering the error values, the present results show that the hydrogen diffusion coefficient is not significantly altered regardless of the increase in the electrolyte concentration, which indicates that the whole electrochemical reaction process is controlled by the interface charge transfer reaction. Interestingly, the values of $D_H$ were three orders of magnitude higher than those reported for the $La_{0.6}Sr_{0.4}FeO_3$ powder in

**Table 2** Exchange current density and diffusion coefficient as a function of the electrolyte concentration

| Parameter/concentration | 6 M | 7.5 M | 8.5 M | 10 M | 12 M |
|---|---|---|---|---|---|
| Polarization resistance (m$\Omega$) | 643.20 (1.1) | 592.66 (0.8) | 557.03 (1.1) | 517.80 (0.9) | 454.10 (1.1) |
| Exchange current density $I_o$ (mA/g) | 39.92 (0.1) | 43.32 (0.05) | 46.10 (0.1) | 49.77 (0.08) | 56.55 (0.1) |
| Hydrogen proton diffusion coefficient $D_H$ ($\times 10^{-14}$ cm$^2$/s) | 1.87 (0.2) | 2.25 (0.3) | 2.09 (0.1) | 2.09 (0.2) | 2.14 (0.1) |

Error values are reported in parenthesis
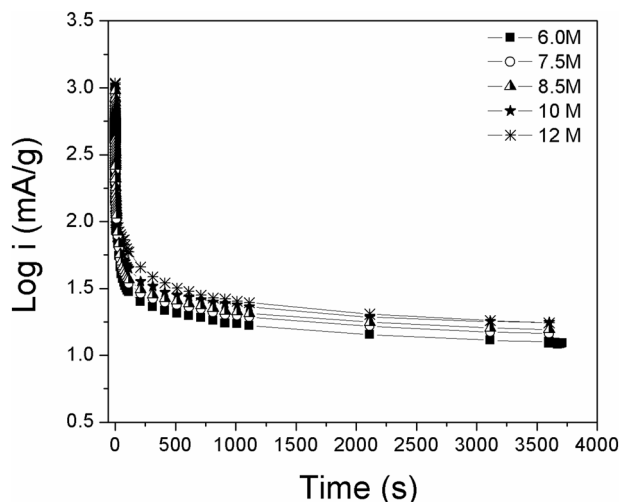
**Fig. 7** Plot of the anodic current density vs. discharge time of the $La_{0.6}Sr_{0.4}Co_{0.2}Fe_{0.8}O_3$ electrode at various electrolyte concentrations and 298 K

previous studies [13], which suggest a significant improvement in the transport properties during the electrochemical process because of the combined effects of the small particle size and Co-doping.

## Conclusions

In this study, the $La_{0.6}Sr_{0.4}Co_{0.2}Fe_{0.8}O_3$ perovskite-type oxide was systematically analyzed in the search for its application as negative electrode material in Ni/oxide rechargeable batteries. The initial powder displayed a perovskite-type structure (orthorhombic phase) with a nanometric particle size distribution. Interestingly, the perovskite-type structure was not significantly affected by the electrochemical charge/discharge process, which presented a small lattice expansion value (0.32%) and the same orthorhombic phase after the 20th cycle. The $La_{0.6}Sr_{0.4}Co_{0.2}Fe_{0.8}O_3$ electrodes also showed electrochemical reversibility and a temperature-dependent discharge capacity. Its initial discharge capacity value was 51.4 mAh $g^{-1}$ at 298 K; it increased, however, to 172 and 462 mAh $g^{-1}$ at 313 and 333 K, respectively. Being similar to the relationship between the discharge capacity and the temperature, the discharge capacity also increased when the electrolyte concentration increased from 6 to 12 M. The improvement in the discharge capacity was associated with the enhanced charge transfer process at the electrode surface due to the increased KOH concentration. This fact was proven by the increase in the exchange current density with the increment of electrolyte concentration. In case of the transport properties, the hydrogen diffusion coefficient showed an improvement when compared with the values reported for non-doped and

micrometric $LaFeO_3$ composition in previous studies. Nevertheless, the values obtained in the present study for the diffusion coefficient (in the order of $10^{-14}$ cm$^2$ s$^{-1}$) still remain below the values reported for intermetallic compounds (in the order of $10^{-10}$ cm$^2$ s$^{-1}$), which, in the present study, can be attributed to the agglomeration of the nanometric particles and poor conductivity of oxides.

Overall, the present results suggest that $La_{0.6}Sr_{0.4}Co_{0.2}Fe_{0.8}O_3$ perovskite-type oxide achieves a better performance at a high electrolyte concentration (12 M) and at high temperatures. Consequently, under this configuration, it can be regarded as a promising electrode material for Ni/oxide rechargeable batteries.

## References

1. Zhao, H., Wu, Q., Hu, S., Xu, H., Rasmussen, C.N.: Review of energy storage system for wind power integration support. Appl. Energy **137**, 545–553 (2015). doi:10.1016/j.apenergy.2014.04.103
2. Manzetti, S., Mariasiu, F.: Electric vehicle battery technologies: from present state to future systems. Renew. Sustain. Energy Rev. **51**, 1004–1012 (2015). doi:10.1016/j.rser.2015.07.010
3. Young, K.H.: Research in nickel/metal hydride batteries. Batteries **2**(4), 1–5 (2016). doi:10.3390/batteries2040031
4. Fetcenko, M.A., Ovshinsky, S.R., Reichman, B., Young, K., Fierro, C., Koch, J., Ouchi, T.: Recent advances in NiMH battery technology. J. Power Sources **165**(2), 544–551 (2007). doi:10.1016/j.jpowsour.2006.10.036
5. Sandrock, G.: A panoramic overview of hydrogen storage alloys from a gas reaction point of view. J. Alloy. Compd. **293**, 877–888 (1999). doi:10.1016/S0925-8388(99)00384-9
6. Zhou, W., Zhu, D., Tang, Z., Wu, C., Huang, L., Ma, Z., Chen, Y.: Improvement in low-temperature and instantaneous high-rate output performance of Al-free AB 5-type hydrogen storage alloy for negative electrode in Ni/MH battery: effect of thermodynamic and kinetic regulation via partial Mn substituting. J. Power Sources **343**, 11–21 (2017). doi:10.1016/j.jpowsour.2017.01.023
7. Zhang, H., Zheng, X., Tian, X., Liu, Y., Li, X.: New approaches for rare earth-magnesium based hydrogen storage alloys. Prog. Nat. Sci. Mater. Int. **27**, 50–57 (2017). doi:10.1016/j.pnsc.2016.12.011
8. Lin, J., Cao, Z., Sun, L., Liang, F., Wu, Y., Wang, L.: Enhanced electrochemical properties of Ti1.4V0.6Ni with Mo2C or WC coating as negative electrodes for Ni-MH battery. J. Alloy. Compd. **695**, 208–214 (2017). doi:10.1016/j.jallcom.2016.10.212

9.  Zhang, L., Ding, Y., Zhao, Y., Du, W., Li, Y., Yang, S., Han, S.: Phase structure and cycling stability of A2B7 superlattice La0.60Sm0.15Mg0.25Ni3.4 metal hydride alloy. Int. J. Hydrogen Energy **41**(3), 1791–1800 (2016). doi:10.1016/j.ijhydene.2015.12.049

10. Ramirez, A.D., Kasa, S.D., Russell, S.D., US Patent No. 9,548,626. Washington, DC: US Patent and Trademark Office, (2017). https://www.google.com/patents/US9548626. Accessed 07 Apr 2017)

11. Trovão, J.P., Machado, F., Pereirinha, P.G.: Hybrid electric excursion ships power supply system based on a multiple energy storage system. IET Electr. Syst. Transp. **6**(3), 190–201 (2016). doi:10.1049/iet-est.2015.0029

12. Meng, T., Young, K.H., Koch, J., Ouchi, T., Yasuoka, S.: Failure mechanisms of nickel/metal hydride batteries with cobalt-substituted superlattice hydrogen-absorbing alloy anodes at 50 C. Batteries. **2**(3), 20 (2016). doi:10.3390/batteries2030020

13. Henao, J., Martinez-Gomez, L.: Review: on rare-earth perovskite-type negative electrodes in nickel–hydride (Ni/H) secondary batteries. Mater. Renew. Sustain. Energy. **6**(2), 7 (2017). doi:10.1007/s40243-017-0091-7

14. Granger, P., Parvulescu, V.I., Kaliaguine, S., Prellier, W.: Perovskites and related mixed oxides: concepts and applications. Wiley, Weinheim (2015)

15. Deng, G., Chen, Y., Tao, M., Wu, C., Shen, X., Yang, H., Liu, M.: Electrochemical properties and hydrogen storage mechanism of perovskite-type oxide $LaFeO_3$ as a negative electrode for Ni/MH batteries. Electrochim. Acta **55**(3), 1120–1124 (2010). doi:10.1016/j.electacta.2009.09.078

16. Wang, Q., Deng, G., Chen, Z., Chen, Y., Cheng, N.: Electrochemical hydrogen property improved in nano-structured perovskite oxide LaFeO3 for Ni/MH battery. J. Appl. Phys. **113**, 053305 (2013). doi:10.1063/1.4790488

17. Pei, Y., Du, W., Li, Y., Shen, W., Wang, Y., Yang, S., Han, S.: The effect of carbon–polyaniline hybrid coating on high-temperature electrochemical performance of perovskite-type oxide LaFeO3 for MH–Ni batteries. Phys. Chem. Chem. Phys. **17**(27), 18185–18192 (2015). doi:10.1039/C5CP02395E

18. Deng, G., Chen, Y., Tao, M., Wu, C., Shen, X., Yang, H.: Electrochemical properties of $La_{1−x}Sr_xFeO_3$ (x = 0.2, 0.4) as negative electrode of Ni–MH batteries. Electrochim. Acta **54**(15), 3910–3914 (2009). doi:10.1016/j.electacta.2009.02.007

19. Deng, G., Chen, Y., Tao, M., Wu, C., Shen, X., Yang, H., Liu, M.: Preparation and electrochemical properties of $La_{0.4}Sr_{0.6}FeO_3$ as negative electrode of Ni/MH batteries. Int. J. Hydrogen Energy **34**(13), 5568–5573 (2009). doi:10.1016/j.ijhydene.2009.04.061

20. Wjihi, S., Sellaoui, L., Bouzid, M., Dhaou, H., Knani, S., Jemni, A., Lamine, A.: B, Theoretical study of hydrogen sorption on $LaNi_5$ using statistical physics treatment: microscopic and macroscopic investigation. Int. J. Hydrogen Energy **42**(5), 2699–2712 (2017). doi:10.1016/j.ijhydene.2016.10.102

21. Nieto, S., Polanco, R., Roque-Malherbe, R.: Absorption kinetics of hydrogen in nanocrystals of $BaCe_{0.95}Yb_{0.05}O_3$-δ proton-conducting perovskite. J. Phys. Chem. C. **111**(6), 2809–2818 (2007). doi:10.1021/jp067389i

22. Wang, Q., Chen, Z., Chen, Y., Cheng, N.: Hui Q, Hydrogen storage in perovskite-type oxides $ABO_3$ for Ni/MH battery applications: a density functional investigation. Ind. Eng. Chem. Res. **51**(37), 11821–11827 (2011). doi:10.1021/ie202284z

23. Jacob, I., Bloch, J.M., Shaltiel, D., Davidov, D.: On the occupation of interstitial sites by hydrogen atoms in intermetallic hydrides: a quantitative model. Solid State Commun. **35**(2), 155–158 (1980). doi:10.1016/0038-1098(80)90234-3

24. Song, M., Chen, Y., Tao, M., Wu, C., Zhu, D., Yang, H.: Some factors affecting the electrochemical performances of $LaCrO_3$ as negative electrodes for Ni/MH batteries. Electrochim. Acta **55**(9), 3103–3108 (2012). doi:10.1016/j.electacta.2010.01.030

25. Tliha, M., Khaldi, C., Mathlouthi, H., Lamloumi, J., Percheron-Guégan, A.: Electrochemical investigation of the iron-containing and no iron-containing AB$_5$-type negative electrodes. J. Alloy. Compd. **440**(1), 323–327 (2007). doi:10.1016/j.jallcom.2006.09.019

26. Deng, G., Chen, Y., Tao, M., Wu, C., Shen, X., Yang, H., Liu, M.: Study of the electrochemical hydrogen storage properties of the proton-conductive perovskite-type oxide $LaCrO_3$ as negative electrode for Ni/MH batteries. Electrochim. Acta **55**(3), 884–886 (2010). doi:10.1016/j.electacta.2009.06.071

27. Ruiz, F.C., Martínez, P.S., Castro, E.B., Humana, R., Peretti, H.A., Visintin, A.: Effect of electrolyte concentration on the electrochemical properties of an AB5-type alloy for Ni/MH batteries. Int. J. Hydrogen Energy. **38**(1), 240–245 (2013). doi:10.1016/j.ijhydene.2012.10.007

28. Li, M., Yang, C.C., Wang, C.C., Wen, Z., Zhu, Y.F., Zhao, M., Jiang, Q.: design of hydrogen storage alloys/nanoporous metals hybrid electrodes for nickel–metal hydride batteries. Scientific reports. **6**, 27601 (2016). doi:10.1038/srep27601

29. Yuan, X., Xu, N.: comparative study on electrochemical techniques for determination of hydrogen diffusion coefficients in metal hydride electrodes. J. Appl. Electrochem. **31**(9), 1033–1039 (2001). doi:10.1023/A:1017995727600